Photoluminescence and resonant Raman scattering in N-doped ZnO thin films

Xiaming Zhu [a], Hui-Zhen Wu [a,b,*], Dong-Jiang Qiu [a], Zijian Yuan [a], Guofen Jin [a],
Jinfang Kong [c], Wenzhong Shen [c]

[a] *Department of Physics, Zhejiang University, Hangzhou 310027, PR China*
[b] *State Key Laboratory of Modern Optical Instrumentations, Zhejiang University, Hangzhou 310027, PR China*
[c] *Department of Physics, Shanghai Jiaotong University, Shanghai 200030, PR China*

ARTICLE INFO

ABSTRACT

A combination of studies on photoluminescence and resonant Raman scattering in N-doped ZnO thin films were carried out at room temperature. In the photoluminescence spectra, a transformation of radiative recombination mechanism from free-exciton to donor–acceptor-pair transition was observed. An enhancement of resonant Raman scattering processes as well as longitudinal optical (LO) phonon overtones up to the sixth order were observed in the Raman spectra. Also, the nature of the 1LO phonon underwent a transformation from a pure $A_1(LO)$ mode to a quasimode with mixed A_1 and E_1 symmetry. The underlying mechanisms accounting for the influences of N doping on the optical properties of ZnO were related to the incorporation of extrinsic defects in the crystal lattice.

1. Introduction

ZnO has attracted great attention in recent years due to its potential applications in optoelectronic and transparent electronic devices [1,2], owing to its direct wide band gap ($E_g \sim 3.37$ eV at room temperature) and large exciton binding energy (~ 60 meV). However, ZnO is still not widely used in practical devices to date because of the difficulty in obtaining stable p-type conductivity in a reproducible way. Until now nitrogen (N) is considered to be the most promising p-type dopant for ZnO due to its similar ionic radius to oxygen and its resistance to forming AX center, a deep defect complex compensating for acceptors [3]. Carrier recombination and phonon scattering processes are important issues in a semiconductor because they have a significant influence on the optical and electrical properties of the material. Two powerful optical characterization techniques, photoluminescence (PL) and Raman spectroscopy, are commonly employed for fast and nondestructive studying carrier recombination and transport processes, respectively. Studies on PL [4] and Raman scattering [5] in N-doped ZnO (ZnO:N) has been reported recently, however, the understanding of fundamental properties in ZnO:N is still relatively incomplete. To further understand the effects of extrinsic defects caused by N doping on the optical and vibrational properties of ZnO, investigations on PL and resonant Raman scattering (RRS) in ZnO:N thin films were carried out at room temperature in this work. Obvious changes in the PL and RRS

properties were observed in ZnO:N, and the underlying mechanisms accounting for the effects of N doping on the optical and vibrational properties of ZnO were discussed in detail.

2. Experiments

The ZnO:N thin films were deposited by a reactive electron beam (e-beam) evaporation system at low temperature [6]. Considering the potential application of ZnO based transparent thin film transistors in the flat-panel display industry [7], amorphous glass was used as substrate in our experiment. High-purity (99.99%) ZnO was used as an evaporation source. During the deposition process, NH_3 gas with 99.999% purity was introduced into the growth chamber as an N-dopant source. Collisions between the high energy e-beams or particles sputtered off the ZnO target and the NH_3 molecules can ionize NH_3 gas partially, and the ionized N atoms are expected to be incorporated into the ZnO lattice thus ZnO:N can be obtained. In the experiment, increasing NH_3 gas partial pressure in the range of 1.0×10^{-2} to 5.0×10^{-2} Pa was employed to acquire ZnO:N with different N concentration. For the comparison of the optical characteristics in N-doped and undoped ZnO, another reference sample without N doping was grown with high-purity (99.999%) O_2 gas. The substrate temperature during deposition was optimized to be 250 °C. After growth, all samples were cut into two parts: one half was retained as an as-grown standard, while the other half was annealed at 500 °C for 30 min in O_2 ambience before characterization. The measured resistivity values of all the annealed ZnO:N samples are nearly 4 orders of magnitude larger than that of the reference sample, which may be attributed to the expectation

* Corresponding author. Department of Physics, Zhejiang University, Hangzhou 310027, PR China. Tel./fax: +86 571 87953885.
E-mail address: hzwu@zju.edu.cn (H.-Z. Wu).

that the addition of NH_3 during growth could compensate oxygen vacancies thus decrease the carrier concentration in ZnO films. The specific growth parameters, film thicknesses, and resistivity values for all ZnO film samples are listed in Table 1.

The ZnO film thicknesses were characterized using a Tencor Alpha Step 200 profilometer by etching a step following film growth. The crystalline structures of the deposited ZnO films were analyzed by a Rigaku D/max-rA X-ray diffractometer with Cu Kα radiation ($\lambda = 0.15406$ nm). The PL measurements were carried out on a Jobin Yvon LabRAM HR 800UV micro-Raman system at room temperature, using the 325 nm line of a He–Cd laser as an excitation source. Non-resonant and resonant Raman measurements were also performed on the Jobin Yvon LabRAM HR 800UV micro-Raman system at room temperature, using the 514.5 nm line of an Ar^+ laser and the 325 nm line of a He–Cd laser as excitation sources, respectively. The number of grating grooves in the Raman spectrometer was 1800 for the visible laser and 2400 for the UV laser. And the laser excitation power was kept low enough to minimize sample heating which could result in thermal-induced Raman peak red shift. All Raman spectra of the ZnO films were recorded in the $z(x,-)\bar{z}$ backscattering configuration, where the z-coordinate is normal to the sample surface. Thus the polarization of the incident light was parallel to the sample surface. The scattered light was not analyzed for its polarization.

3. Results and discussion

The X-ray diffraction (XRD) patterns of the as-grown and post-deposition annealed ZnO:N sample N2 are shown in Fig. 1, and the XRD curves of the as-grown and annealed undoped ZnO reference sample O2 are plotted in the inset. For the as-grown undoped ZnO, an intense peak at 34.56° was observed, which corresponds to the (002) diffraction peak of ZnO. Its full width at half maximum (FWHM) value decreased from 0.321° to 0.308° after annealing, implying that the film quality was improved by post-growth heat treatment. According to the Scherrer's formula, the average grain size estimated from the (002) peak is about 25.9 nm in the as-grown ZnO film, and it increases to 27.0 nm after annealing. The slight shift in the peak position 2θ toward lower angle upon annealing may be attributed to the partial release of stress in the film.

For the as-grown ZnO:N, the dominant (002) diffraction peak of ZnO reveals that the ZnO:N film deposited on amorphous glass at low temperature still shows a preferred c-axis orientation. Larger FWHM values of the (002) peaks were observed in both the as-grown and annealed ZnO:N compared with those of the undoped ZnO, respectively. The broadening of the (002) peak caused by N doping can be interpreted as due to the incorporation of extrinsic defects, e.g. substitutional N atoms and/or N–H complexes [8,9] on O sites, in the ZnO lattice. And the slightly larger 2θ values for ZnO:N may arise from the fact that the bond length of Zn–N (1.88 Å) [3] is smaller than that of Zn–O (1.93 Å). The average grain size is about 20.1 nm in the as-grown ZnO:N film, and it increases to 22.6 nm after annealing.

Fig. 2 shows the room temperature PL spectra of the as-grown undoped and N-doped ZnO film samples. An intense ultraviolet (UV)
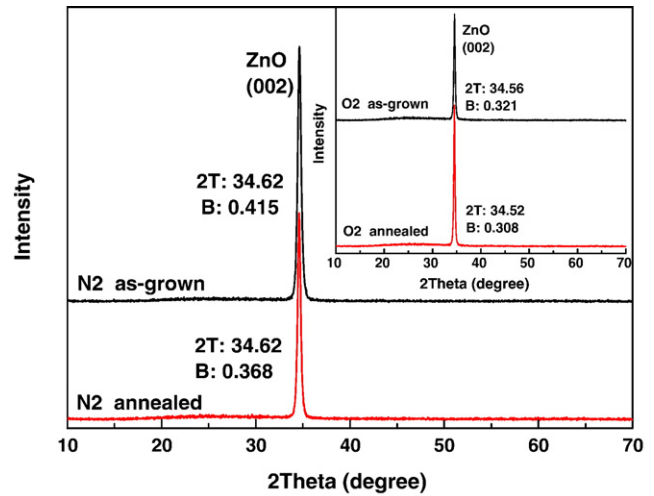

Fig. 1. The X-ray diffraction (XRD) spectra of the as-grown and post-deposition annealed N-doped ZnO sample (N2), and the inset shows the XRD patterns of the as-grown and post-deposition annealed undoped ZnO reference sample (O2), where the "2T" denotes the peak center and the "B" denotes the full width at half maximum.

peak at 3.286 eV (377.4 nm) was observed from the undoped ZnO. This peak was considered as a superimposition of multiple peaks due to the convergence of the A- and B-exciton peaks, and the coupling of the 1LO-phonon replica with the line broadening of each of these peaks at room temperature [10], so it can be attributed to a free-exciton related transition. For the ZnO:N sample N1, with the lowest NH_3 partial pressure in the growth process, the UV peak appeared at 3.280 eV (378.0 nm). Its peak position red-shifted 6 meV and its intensity decreased by 75% compared to those of the undoped ZnO, respectively. The origin of the peak is still related to the free excitonic transition, and the slight shift of the peak may stem from the strain induced by N doping, resulting energy change of the band structure. As the NH_3 partial pressure was increased further, the UV peak became rather weak and broad, and its peak position red-shifted gradually to around 3.0 eV. According to recent reports that substitutional nitrogen on oxygen site (N_O) induces a shallow acceptor level which is about 165 meV above valence band [11] and Zn_i–N_O complex is a shallow donor at about 30 meV [12], the weak broad PL line at about 3.0 eV can be attributed to a donor–acceptor-pair (DAP) recombination, i.e., related to the Zn_i–N_O shallow donor

Table 1
Deposition parameters for ZnO thin films on amorphous glass at 250 °C by e-beam evaporation system.

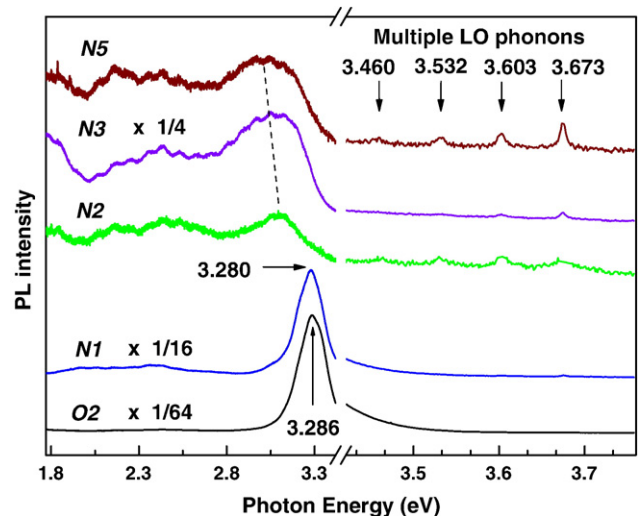| Sample	Growth ambience	Partial pressure/Pa	Thickness/nm	Resistivity after annealing/$\Omega \cdot$cm
O2	O_2	2.0×10^{-2}	220	1.68×10^{-1}
N1	NH_3	1.0×10^{-2}	470	2.37×10^3
N2	NH_3	2.0×10^{-2}	345	6.96×10^5
N3	NH_3	3.0×10^{-2}	220	4.18×10^5
N5	NH_3	5.0×10^{-2}	330	1.65×10^6

Fig. 2. Room temperature PL spectra of the as-grown ZnO samples, and the high energy region also shows resonant LO phonon peaks due to 325 nm Raman excitation.

and N_O acceptor. The weak and broad luminescence band in the range of 2.0 to 2.7 eV in ZnO:N has previously been attributed to deep level defects such as oxygen vacancies (V_O) in the crystal structure [10]. In addition, it is interesting to note that several evenly spaced peaks were observed at 3.460, 3.532, 3.603, and 3.673 eV, with intervals of about 71 meV, on the high energy side of the PL spectra for ZnO:N. These peaks were attributed to multiple longitudinal optical phonon RRS modes excited by the 325 nm laser line.

It has been established that the PL intensity I can be expressed as [13,14]

$$I = \eta I_0^{\alpha} \tag{1}$$

where I_0 is the excitation laser power, η is the emission efficiency, and exponent α is a coefficient associated with radiative recombination mechanism. For excitonic recombination, $1 < \alpha < 2$, and for DAP transition, $\alpha < 1$ [13]. Furthermore, exciton lifetime is an important parameter related to material quality, becoming longer as crystal quality improves, and efficiency of radiative recombination is strongly related to lifetime of particular transition. For the comparison of the PL features in N-doped and undoped ZnO, identical measurement conditions were employed for each film sample. As can be seen in Fig. 2, the obvious decrease in the UV emission intensity for the ZnO:N sample N1, compared to that of the reference sample O2, can be interpreted as due to the degradation of the ZnO crystal quality caused by N doping, which can result in the decrease of exciton lifetime thus reduce the emission efficiency of the excitonic radiative recombination η. However, the further decrease in the PL intensity for samples N2, N3, and N5, compared to that of the sample N1, mainly arises from the different recombination origins, since the exponent coefficient α for the DAP transition is smaller than that for the excitonic one.

The würtzite ZnO belongs to the space group C_{6v}^4 with two formula units in the primitive cell, and group theory predicts the zone-center optical modes are A_1, $2B_1$, E_1 and $2E_2$ [15]. The A_1 and E_1 modes are polar and Raman and infrared active, while the two E_2 modes (E_2^{low}, E_2^{high}) are nonpolar and Raman active only. The vibrations of the polar A_1 and E_1 modes can polarize the unit cell, which creates a long-range electrostatic field splitting the polar modes into longitudinal optical (LO) and transverse optical (TO) components. The B_1 modes are Raman and infrared inactive (silent modes).

Fig. 3 shows the Raman scattering (RS) spectra of the as-grown N-doped and undoped ZnO, excited by the 514.5 nm laser line (2.410 eV). The energy of the excitation photon is lower than the E_g

Fig. 3. Room temperature non-resonant Raman scattering spectra of the as-grown undoped ZnO sample (O2) and the N-doped ZnO sample (N5) excited by the 514.5 nm laser line.

value of ZnO, and accords with the non-resonant RS condition. According to the well-known Raman selection rules, only E_2 and A_1(LO) modes, determined at 437 and 574 cm^{-1} for single crystal ZnO [16], respectively, can be observed in the backscattering geometry employed in our measurements. As can be seen in both spectra, a broad peak ranging from 500 to 740 cm^{-1} appeared at about 559 cm^{-1}, which was excited from the glass substrate as a result of the high transmittance for the visible laser line in the ZnO thin film. For the undoped ZnO reference sample O2, the E_2^{high} mode at 437 cm^{-1} was distinctly observed, but the A_1(LO) mode expected at 574 cm^{-1} was too weak to be observed due to its rather small scattering cross section [17] and the interference from the strong background signal. For the ZnO:N sample N5, three anomalous Raman modes at 275, 510, and 577 cm^{-1} were observed except for the E_2^{high} mode. Based on both the theoretical and experimental studies, the Raman mode at 275 cm^{-1} was attributed to the localized vibration of Zn atoms, where parts of their first nearest neighbor O atoms are replaced by N atoms in the ZnO lattice [18]. Moreover, the intensity of the mode was found to be correlated linearly with the N concentration in both the N-doped and N$^+$-implanted ZnO [5,18]; so the N concentration in the ZnO:N sample N5 grown with the highest NH$_3$ partial pressure can be estimated to be approximately 10^{18} cm^{-3} by the occurrence of the mode. The anomalous mode at 510 cm^{-1} only appeared in ZnO:N and can be interpreted as due to the presence of N atoms in the ZnO lattice [19,20]. The Raman mode at around 577 cm^{-1}, which just falls between the A_1(LO) (574 cm^{-1}) and E_1(LO) (590 cm^{-1}) modes [16] of single crystal ZnO, may be interpreted as an LO quasimode with mixed A_1 and E_1 symmetry induced by defects, which will be discussed in detail later.

RRS [21,22] is a well-known phenomenon that occurs when the excitation energy is close to or larger than the optical gap of a semiconductor. In this case, the virtual states participating in the scattering processes are substituted by real electronic states. This leads to an enhancement of the scattering cross sections for phonons that couple to electrons via the Fröhlich interaction. Fig. 4(a) represents the room temperature RRS spectra of the as-grown and post-deposition annealed undoped ZnO, excited by the 325 nm laser line (3.815 eV). Compared to the non-resonant RS spectra, as shown in Fig. 3, the LO phonon was enhanced greatly which implied the strong contribution of Fröhlich interaction to the LO phonon scattering efficiency [23]. For the as-grown sample, three evenly spaced Raman modes dominated at around 569, 1138, and 1708 cm^{-1}, which can be attributed to the nth-order ($n = 1$, 2, 3) A_1(LO) phonons of ZnO, respectively. Interestingly, the intensities of these modes decreased evidently after annealing. The enhancement of the A_1(LO) mode, compared to that of the annealed one, may arise from the point defects existing in the as-grown film which can contribute to the RRS processes via defect-induced Raman scattering. In addition, phonon peak red shifts were clearly observed for the A_1(LO) and $2A_1$(LO) modes in the as-grown sample, compared to those of the annealed one, respectively. Considering the previous XRD results that the (002) peak of the as-grown ZnO film shifted slightly upon annealing, as shown in the inset of Fig. 1, the red shifts observed in the Raman peaks may be caused by the tensile stress which probably exists in the as-grown ZnO film deposited on amorphous glass. The weak mode at 321 cm^{-1} corresponds to a second-order Raman scattering process, which has been proven to be the $E_2^{high} - E_2^{low}$ difference mode [16].

Fig. 4(b) shows the room temperature multiphonon RRS spectra of the four as-grown ZnO:N samples under the 325 nm excitation. The RRS feature of the as-grown ZnO:N sample N1, with the lowest NH$_3$ partial pressure in the growth process, was quite similar to that of the undoped ZnO. Three-order LO phonon modes and a sharp rise in the scattering intensity, which is attributed to the strong PL signal excited from ZnO, were observed in the whole spectrum. With the NH$_3$ partial pressure further increasing, the order number of the RRS reached up to six and the intensities of the 1LO phonons enhanced evidently. The 1LO phonons of the as-grown ZnO:N were fitted by Lorentzian line
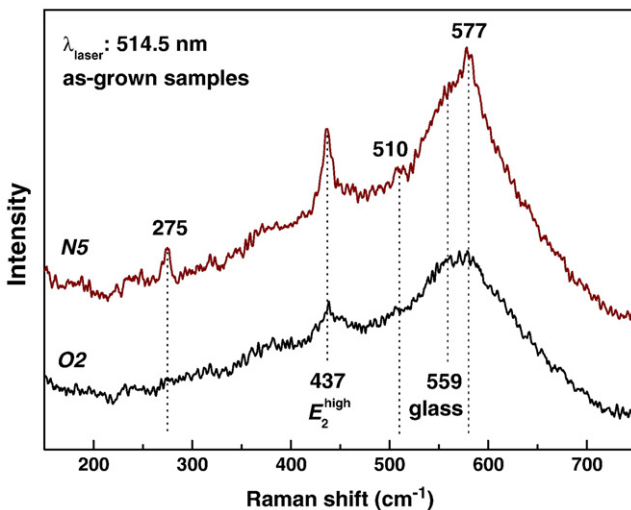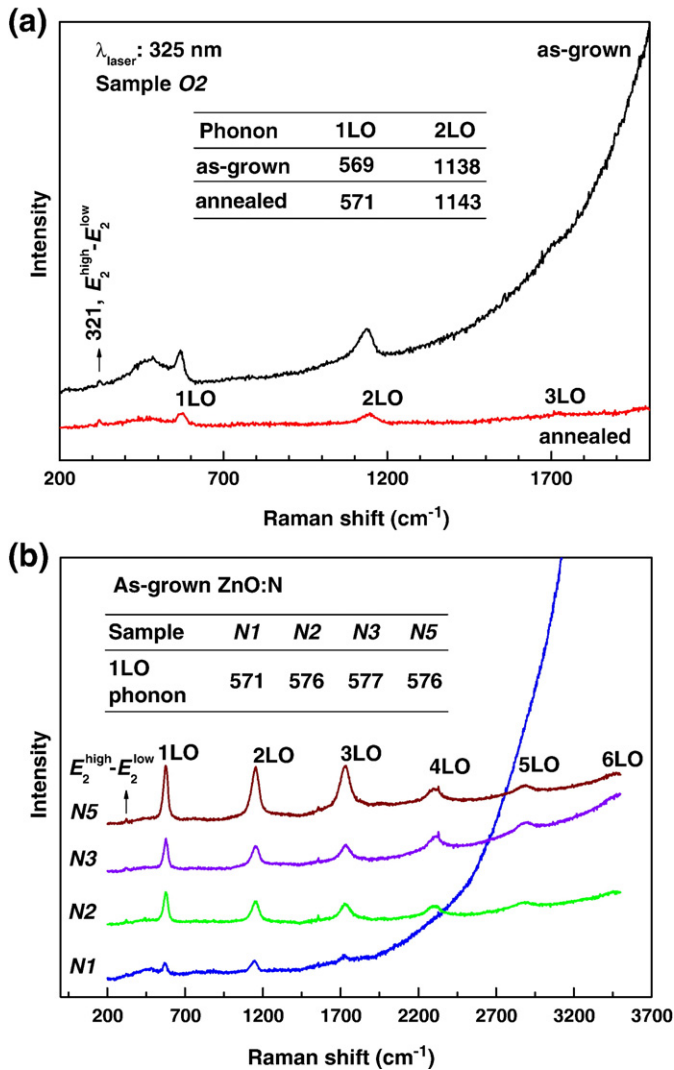
Fig. 4. Room temperature resonant Raman scattering spectra of (a) the as-grown and post-deposition annealed undoped ZnO and (b) the four as-grown ZnO:N samples with the 325 nm excitation.

shapes and the peak centers were determined at 571, 576, 577, and 576 cm^{-1} for samples N1, N2, N3, and N5, respectively.

The underlying mechanism accounting for the intensity enhancements of the 1LO phonons in ZnO:N could be understood in the following way: In ZnO:N, impurities (extrinsic defects) were incorporated into the ZnO lattice, such as substitutional N atoms and/or N–H complexes [8,9] on O sites, which may cause the breakdown of the translation symmetry of the lattice. Thus the momentum conservation is relaxed and phonons with wave vectors throughout the whole Brillouin zone can participate in the Raman scattering [24]. Since the intensity of the Raman scattering for the Fröhlich interaction mechanism is proportional to the magnitude of phonon wave vector [25], those larger wave vectors can greatly enhance the intraband Fröhlich interaction [26,27] and therefore increase the corresponding scattering cross section. As the NH$_3$ partial pressure increases in the growth process, more impurities and defects were expected to be formed in the ZnO lattice and so the 1LO phonons enhanced further. Moreover, the PL background signal decreased evidently with the NH$_3$ partial pressure further increasing, which was in agreement with the previous PL results, as shown in Fig. 2. And the enhancements of the multiphonon RRS processes in ZnO:N may be related to the sharp decrease in the PL intensity, which offers better conditions for observing higher order overtones.

As can be seen in Fig. 4(b), the 1LO mode of the sample N1 locates at 571 cm^{-1}, which is quite close to that of the reference sample O2 (569 cm^{-1}). However, the 1LO modes of the other ZnO:N samples blue-shifted to similar values of 576 cm^{-1}. The observable difference between the two phonon peak positions for ZnO:N implies that they probably have different origins. As mentioned above, only the polar A$_1$ (LO) mode dominates in the RRS spectrum in a backscattering geometry with the incident light parallel to the c axis of single crystal ZnO. For the as-grown ZnO:N sample N1, the PL intensity was really strong whereas the 1LO phonon intensity was rather weak, which demonstrated that few impurities and defects were formed in the film and the würtzite structure was still maintained well. So the 1LO mode of sample N1 can be interpreted as the A$_1$(LO) mode of ZnO. With the NH$_3$ partial pressure further increasing, more impurities and defects may be formed in the ZnO:N film as indicated by the above discussions, which can induce the lattice disorder thus the degradation of the crystal quality. As shown in Fig. 1, the FWHM value of the (002) peak for the as-grown ZnO:N sample N2 (0.415°) was much larger than that of the as-grown reference sample O2 (0.321°), which also indicated that the c-axis orientation of some crystallites may deviate from the direction normal to the film surface. From a recent report [28], a quasimode occurs in Raman scattering if the phonon propagating direction does not overlap exactly with the crystal symmetry axes (a or c axes of the würtzite structure). According to the Loudon's model [29], the LO quasimode has mixed A$_1$ and E$_1$ symmetry and propagates between the a and c axes in würtzite crystals. And so the 1LO mode observed at 576 cm^{-1} can be attributed to an LO quasimode with mixed A$_1$ and E$_1$ symmetry.

4. Conclusion

In summary, ZnO:N thin films have been deposited on amorphous glass at low temperature by e-beam evaporation, with an increasing partial pressure of the doping gas NH$_3$ during growth. The XRD results indicated that the ZnO:N films grown on glass still maintained c axis orientation preferred würtzite structure. The room temperature PL and RS properties in ZnO:N films were studied systematically. A transformation of radiative recombination mechanism from free-exciton to donor–acceptor-pair transition was observed in the PL spectra of ZnO:N. The comparison of the non-resonant RS spectra between N-doped and undoped ZnO distinctly showed the incorporation of N atoms in the ZnO lattice by NH$_3$ doping. Enhancements of the RRS processes and LO phonon overtones up to the sixth order were observed in ZnO:N at room temperature. And the nature of the 1LO phonon underwent a transformation from a pure A$_1$(LO) mode to a quasimode with mixed A$_1$ and E$_1$ symmetry. The underlying mechanisms accounting for the observed phenomena were found to be related to the extrinsic defects incorporated into the ZnO lattice by N doping.

References

[1] D.C. Look, Mater. Sci. Eng. B 80 (2001) 383.
[2] J.F. Wager, Science 300 (2003) 1245.
[3] C.H. Park, S.B. Zhang, S.H. Wei, Phys. Rev. B 66 (2002) 073202.
[4] H.B. Ye, J.F. Kong, W.Z. Shen, J.L. Zhao, X.M. Li, J. Phys. D 40 (2007) 5588.
[5] A. Kaschner, U. Haboeck, M. Strassburg, M. Strassburg, G. Kaczmarczyk, A. Hoffmann, C. Thomsen, A. Zeuner, H.R. Alves, D.M. Hofmann, B.K. Meyer, Appl. Phys. Lett. 80 (2002) 1909.
[6] H.Z. Wu, K.M. He, D.J. Qiu, D.M. Huang, J. Cryst. Growth 217 (2000) 131.

[7] H.Z. Wu, J. Liang, G.F. Jin, Y.F. Lao, T.N. Xu, IEEE Trans. Electron. Devices 54 (2007) 2856.
[8] X. Li, B. Keyes, S. Asher, S.B. Zhang, S.-H. Wei, T.J. Coutts, S. Limpijumnong, C.G. Van de Walle, Appl. Phys. Lett. 86 (2005) 122107.
[9] S.J. Jokela, M.D. McCluskey, Phys. Rev. B 76 (2007) 193201.
[10] U. Ozgur, Y.I. Alivov, C. Liu, A. Teke, M.A. Reshchikov, S. Dogan, V. Avrutin, S.J. Cho, H. Morkoc, J. Appl. Phys. 98 (2005) 041301.
[11] B.K. Meyer, H. Alves, D.M. Hofmann, W. Kriegseis, D. Forster, F. Bertram, J. Christen, A. Hoffmann, M. Strassburg, M. Dworzak, U. Haboeck, A.V. Rodina, Phys. Status Solidi B 241 (2004) 231.
[12] D.C. Look, G.C. Farlow, P. Reunchan, S. Limpijumnong, S.B. Zhang, K. Nordlund, Phys. Rev. Lett. 95 (2005) 225502.
[13] T. Schmidt, K. Lischka, W. Zulehner, Phys. Rev. B 45 (1992) 8989.
[14] L. Bergman, J.L. Morrison, X.B. Chen, J. Huso, H. Hoeck, Appl. Phys. Lett. 88 (2006) 023103.
[15] T.C. Damen, S.P.S. Porto, B. Tell, Phys. Rev. 142 (1966) 570.
[16] R. Cusco, E. Alarcon-Llado, J. Ibanez, L. Artus, J. Jimenez, B. Wang, M.J. Callahan, Phys. Rev. B 75 (2007) 165202.
[17] N. Ashkenov, B.N. Mbenkum, C. Bundesmann, V. Riede, M. Lorenz, D. Spemann, E.M. Kaidashev, A. Kasic, M. Schubert, M. Grundmann, G. Wagner, H. Neumann, V. Darakchieva, H. Arwin, B. Monemar, J. Appl. Phys. 93 (2003) 126.
[18] J.B. Wang, H.M. Zhong, Z.F. Li, W. Lu, Appl. Phys. Lett. 88 (2006) 101913.
[19] L. Artus, R. Cusco, E. Alarcon-Llado, G. Gonzalez-Diaz, I. Martil, J. Jimenez, B. Wang, M. Callahan, Appl. Phys. Lett. 90 (2007) 181911.
[20] F. Friedrich, N.H. Nickel, Appl. Phys. Lett. 91 (2007) 111903.
[21] J.F. Scott, T.C. Damen, W.T. Silfvast, R.C.C. Leite, L.E. Cheesman, Opt. Commun. 1 (1970) 397.
[22] J.F. Scott, Phys. Rev. B 2 (1970) 1209.
[23] R.M. Martin, T.C. Damen, Phys. Rev. Lett. 26 (1971) 86.
[24] R.P. Wang, G. Xu, P. Jin, Phys. Rev. B 69 (2004) 113303.
[25] J. Menendez, M. Cardona, Phys. Rev. B 31 (1985) 3696.
[26] W.H. Sun, S.J. Chua, L.S. Wang, X.H. Zhang, J. Appl. Phys. 91 (2002) 4917.
[27] V.V. Ursaki, I.M. Tiginyanu, V.V. Zalamai, E.V. Rusu, G.A. Emelchenko, V.M. Masalov, E.N. Samarov, Phys. Rev. B 70 (2004) 155204.
[28] L. Bergman, X.B. Chen, J. Huso, J.L. Morrison, H. Hoeck, J. Appl. Phys. 98 (2005) 093507.
[29] R. Loudon, Adv. Phys. 13 (1964) 423.